EPJ Web of Conferences **99**, 04002 (2015)
DOI: 10.1051/epjconf/20159904002

Primary CR energy spectrum and mass composition by the data of Tunka-133 array

V.V. Prosin[1,a], S.F. Berezhnev[1], N.M. Budnev[2], A. Chiavassa[3], O.A. Chvalaev[2], A.V. Dyachok[2], S.N. Epimakhov[4], O.A. Gress[2], T.I. Gress[2], N.N. Kalmykov[1], N.I. Karpov[1], E.N. Konstantinov[2], A.V. Korobchenko[2], E.E. Korosteleva[1], V.A. Kozhin[1], L.A. Kuzmichev[1,2], B.K. Lubsandorzhiev[5], N.B. Lubsandorzhiev[1], R.R. Mirgazov[2], R.D. Monkhoev[2], E.A. Osipova[1], A.L. Pakhorukov[2], M.I. Panasyuk[1], L.V. Pankov[2], E.G. Popova[1], V.S. Ptuskin[7], Y.A. Semeney[2], A.A. Silaev[1], A.A. Silaev (jun.)[1], A.V. Skurikhin[1], C. Spiering[6], L.G. Sveshnikova[1], and A.V. Zagorodnikov[2]

[1] Skobeltsyn Institute of Nuclear Physics, Lomonosov Moscow State University, Moscow, Russian Federation
[2] Institute of Applied Physics, Irkutsk State University, Irkutsk, Russian Federation
[3] University of Turin, Italy
[4] Institute fur Experimentalphysik, University of Hamburg, Germany
[5] Institute of Nuclear Research, Russian Academy of Sciences, Moscow, Russian Federation
[6] DESY Zeuthen, Germany
[7] Pushkov Institute of Terrestrial Magnetism, Ionosphere and Radio Waves Distribution, Russian Academy of Sciences, Moscow, Russian Federation

Abstract. The Cherenkov light array for the registration of extensive air showers (EAS) Tunka-133 collected data during 5 winter seasons from 2009 to 2014. The differential energy spectrum of all particles and the dependence of the average maximum depth on the energy in the range of $6 \cdot 10^{15}$–10^{18} eV measured for 1540 hours of observation are presented.

1. Introduction

The EAS Cherenkov light array Tunka-133 with $\sim 3\,\mathrm{km}^2$ geometric area has been operating since 2009 [1]. Five winter seasons of data acquisition ($\sim 10^7$ triggers) and high quality of information allowed us to reconstruct the primary energy spectrum and the mean mass composition in the energy range $6 \cdot 10^{15}$–10^{18} eV. This energy range is the most important for understanding the transition from Galactic to extragalactic cosmic rays (CR).

2. The Tunka-133 array

The Tunka-133 array is located in the Tunka Valley (50 km from Lake Baikal) on the banks of the Irkut river, at an altitude of 670 m a.s.l. The Tunka-133 array consists of 175 optical detectors using PMTs with a hemispherical photocathode of 20 cm diameter. The detectors are grouped into 19 clusters each with seven detectors – six hexagonally arranged detectors and one in the center. The distance between the detectors in the cluster is 85 m (see Fig. 1).

An optical detector (see Fig. 1) consists of a 50 cm diameter metallic cylinder, containing a PMT. The container window is directed to the zenith and covered with plexiglass heated against hoar-frost and dew. The detector is equipped with a remotely controlled lid protecting the PMT from sunlight and precipitation.

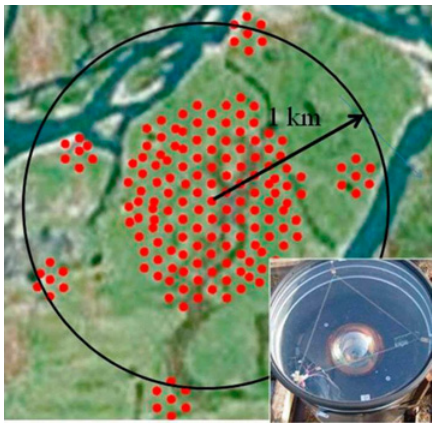

Figure 1. Layout of the Tunka-133 array and front view of an optical detector.

The detector efficiency vs. the zenith angle was presented in [2]. The decrease of the sensitive area with increasing zenith angle and the shadowing of PMT cathode by the container window edge leads to a decrease of acceptance from 1 to about 0.8 at an angle of 34° and to about 0.45 at an angle of 45°. The acceptance curve is used to correct the Cherenkov light flux for inclined events.

To check the calculated efficiency vs. zenith angle curve we analyse the zenith angle distribution of the recorded EAS with energies above a fixed value. The resulting zenith angle distribution of EAS with energies

[a] e-mail: v-prosin@yandex.ru

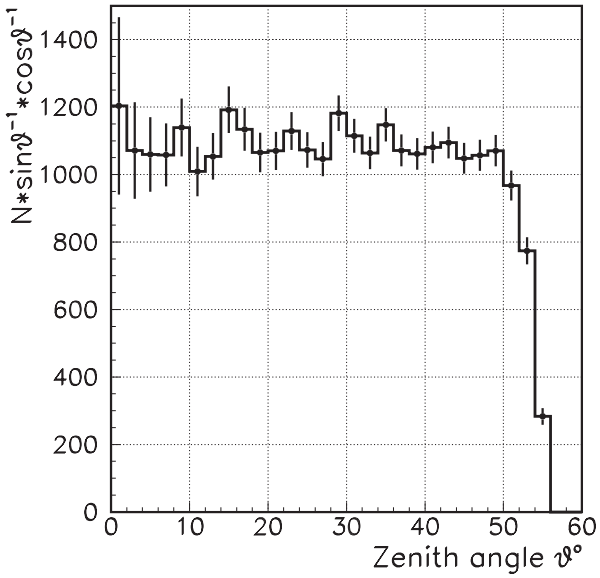

Figure 2. Zenith angle distribution for showers with fixed primary energy.

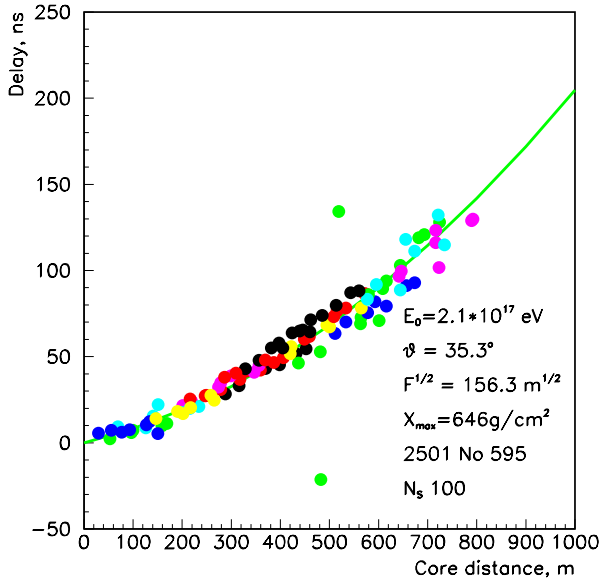

Figure 3. An example of the experimental EAS time front reconstruction for a single event.

larger than 15 PeV is presented in Fig. 2. The distribution is uniform until 50°.

The PMT output pulses are sent via 95 m coaxial cable RG58 to the cluster electronics box, placed in the center of the cluster. The minimum pulse FWHM after passing through the coaxial cable is about 20 ns. The dynamic range of the amplitude measurement is about $3 \cdot 10^4$. This is achieved by means of two channels for each detector extracting the signals from the anode and from the intermediate dynode of the PMT with different additional amplification factors. In the cluster electonics box each pulse is digitized by a 200 MHz 12 bit sampling FADC board. Data from the cluster electronics box is sent to the DAQ center via optical fiber line.

The amplitude calibration of the detectors was carried out in two steps similar to that used in the previous Tunka-25 experiment. The details are described in [3].

3. EAS parameters reconstruction

3.1. Experimental data

The Cherenkov light array Tunka-133 operates on clear moonless nights every year from October until the beginning of April. During other seasons nights are too short and weather conditions are mostly unsatisfactory.

Data for 262 nights of observation was collected during 5 winter seasons of 2009-2014. The trigger condition was a coincidence of pulses in 3 detectors of a cluster inside a time gate of 0.5μ s. The mean trigger rate was about 2 Hz. About 10^7 trigger events for 1540 hours during these nights were accumulated.

The Tunka-133 data were processed using the original codes, in which all fitting and conversion functions were obtained from the analysis of events simulated by CORSIKA for the energy range 10^{15}–10^{18} eV. The details were described in [4].

3.2. Arrival direction

The shower arrival direction (characterized by zenith θ and azimuth ϕ angles) is reconstructed by fitting the measured delays with a curved shower front: $\Delta T = T_i - T_f = R \cdot (R + 500)/(c \cdot F)$, where T_f – estimated delay for a plane front, R – the perpendicular distance from the shower axis in meters, c – the speed of light, F is a variable parameter. This approximate formula is derived from the analysis of CORSIKA simulated showers. The formula, on the one hand, has a non-zero value of the derivative at $R = 0$ (conical shape, typical for Cherenkov radiation at short distances from the axis) and on the other hand, has only one shape parameter which is essential for processing relatively small showers. An example of the experimental EAS front reconstruction during the measurement of the arrival direction is shown in Fig. 3.

The accuracy of the arrival direction reconstruction using the curve fitting front is better than in the plane model, but this method demands a preliminary estimate of the EAS core position.

3.3. Core position

The reconstruction of the EAS core position is performed by fitting measured amplitudes A_i with an amplitude distance function (ADF), presented in [4].

The ADF has four different parametrizations in the different ranges of core distance. But all four parameters are related to a single parameter of the ADF shape – the steepness b_A.

The ADF steepness parameter b_A is treated as an independent variable during the minimisation of the adequate functional. But, if two other independent variables of the core coordinates define the core position far from the dense part of the array, b_A is treated as a fixed parameter. It's value is derived from the value of X_{max}, obtained from the mean width, τ_{eff}, of Cherenkov light pulses at a distance of 400 m to the core $\tau(400)$.

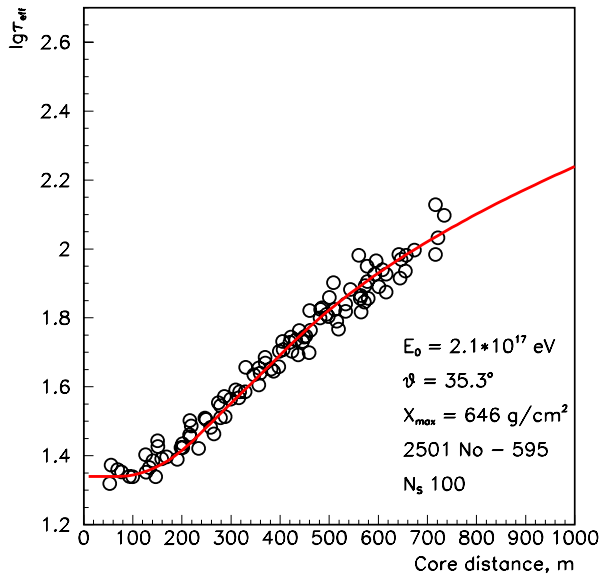

Figure 4. An example of experimental Cherenkov light pulse width as a function of EAS core distance.

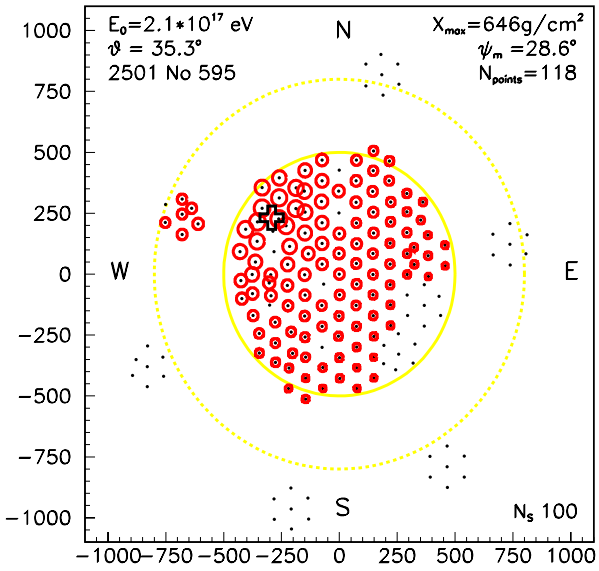

Figure 5. An example of experimental EAS core reconstruction. The radius of each station circle is proportional to $log\,Q_i$.

The connection τ_{eff} vs. X_{max} and b_A vs. X_{max} has been obtained and discussed in [4]. An example of the individual experimental dependance of τ_{eff} on the core distance used for $\tau(400)$ reconstruction is shown in Fig. 4.

3.4. Energy reconstruction

As a measure of energy we use the Cherenkov light flux density at a core distance of 200 m – $Q(200)$. Reconstruction of $Q(200)$ is made by fitting the measured values of Q_i with the lateral distribution function (LDF) [5].

The connection between the EAS energy, E_0, and $Q(200)$ can be expressed by the following formula:

$$E_0 = C \cdot Q(200)^g. \qquad (1)$$

It was found from CORSIKA simulations that, for the energy range of 10^{14}–10^{18} eV, the zenith angle range of 0°–45° and a complex composition consisting of equal contribution of protons and iron nuclei, the value of the index g is 0.94. The real composition is not far from this assumption. Measurements of X_{max} show that the mean value of lnA is about 2 ± 0.5 in the whole energy range 10^{14}–10^{18} eV.

To reconstruct the EAS energy from the Cherenkov light flux one needs to know the absolute sensitivities of the Cherenkov detectors and the atmosphere transparency. To avoid these problems, the method of normalizing the integral energy spectrum to a reference spectrum is used. The reference energy spectrum was measured by the QUEST experiment [6,7]. The integral energy spectrum obtained for each night of the Tunka-133 operation is normalised to that reference spectrum.

An example of core reconstruction is presented in Fig. 5. The adequate ADF and LDF functions for this event are shown in Fig. 6.

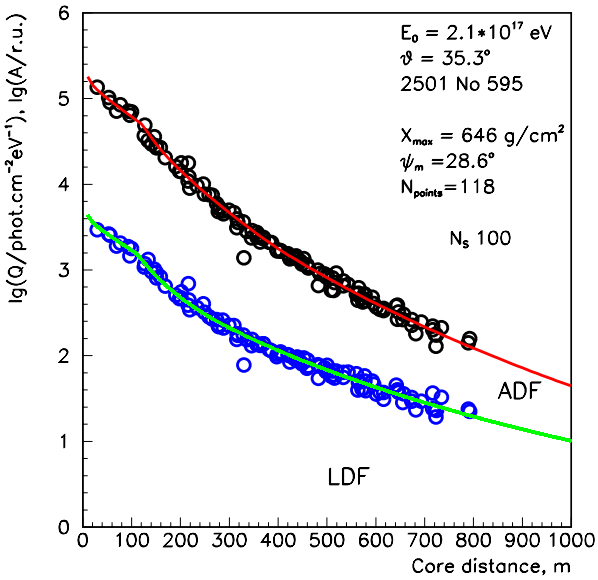

Figure 6. An example of experimental EAS pulse amplitudes fitting with ADF and the resulting LDF.

3.5. Experimental evaluation of the accuracy of the EAS main parameters

The experimental evaluation of errors of the reconstructed EAS parameters is interesting because of the complexity of the simulation of all the possible measurement errors. Simultaneous recording of showers by two independent arrays allows us to make such an evaluation.

We applied a method of partitioning the total array into two independent sub-arrays one being the odd detectors, and the other the even detectors. Then the EAS parameters have been reconstructed for the same event by the data of these two sub-arrays. All the events recorded during the winter of 2013–2014 have been used for such a procedure. The results of comparing the same event parameters

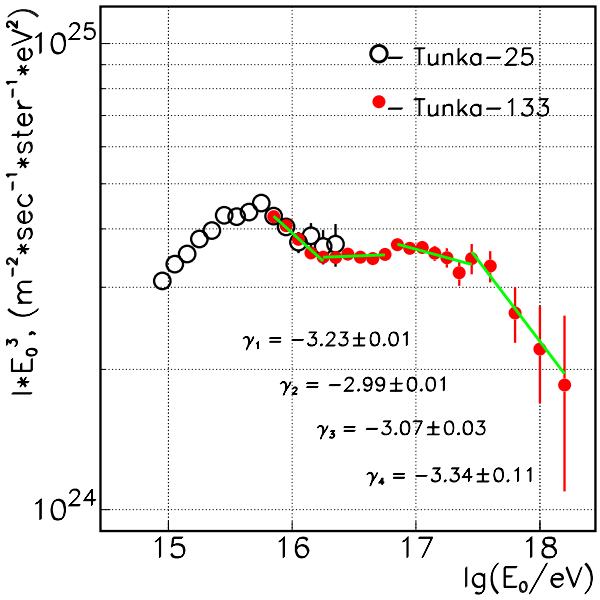

Figure 7. Differential primary cosmic rays (CR) energy spectrum.

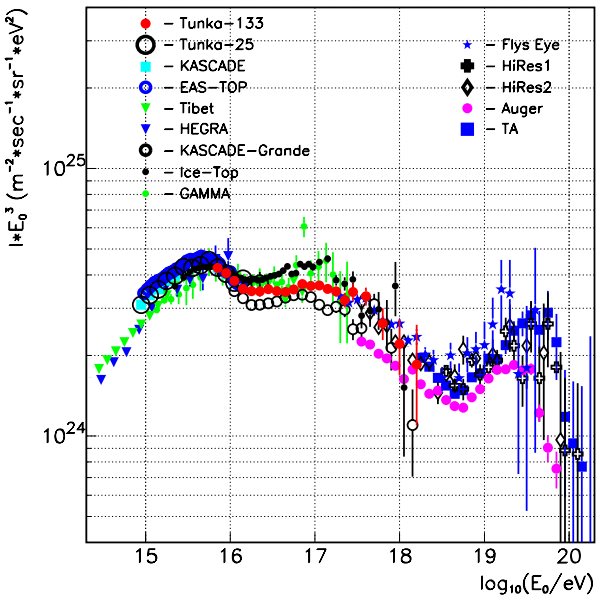

Figure 8. Comparison of energy spectra obtained at Tunka Valley with some other experimental results.

reconstructed by the data of different sub-arrays are as follows.

An average difference between core positions is $\overline{\Delta R} = 8$ m for the dense part of the array of radius 450 m and for energy $E_0 \geq 10^{16}$ eV. The standard deviation of the ratio of energies reconstructed by the data of different sub-arrays is 8%. For energies $E_0 \geq 3 \cdot 10^{16}$ eV the average difference between core positions is $\overline{\Delta R} = 6$ m, and the standard deviation of the ratio of energies reconstructed by the data of different sub-arrays is 4%.

For showers with core positions within a circle of radius 800 m and energy $E_0 \geq 5 \cdot 10^{16}$ eV, the average difference between core positions is $\overline{\Delta R} = 13$ m, and the standard deviation of the ratio of energies reconstructed by the data of different sub-arrays is 12%.

4. Energy spectrum

To construct the Tunka-133 spectrum events were selected for zenith angles $\theta \leq 45^\circ$ with the core position inside a circle of radius $R_c \leq 450$ m for energies $E_0 < 5 \cdot 10^{16}$ eV, and a circle of radius $R_c < 800$ m for showers with energy $E_0 \geq 5 \cdot 10^{16}$ eV. Comparison of the spectra for these two effective areas showed that starting from the above mentioned energy, spectra within the error bars are the same, but the event statistics in the second round is 3 times more which is essential for energies $E_0 \geq 10^{17}$ eV.

The efficiency of shower selection inside a circle with $R_c \leq 450$ m reaches 100% for energies $E_0 \geq 6 \cdot 10^{15}$ eV. The total number of events above this energy is 270.000. About 3.000 events, selected within a circle with $R_c < 800$ m, have $E_0 \geq 10^{17}$ eV.

The resulting differential Tunka-133 energy spectrum is shown in Fig. 7 together with the previous spectrum of Tunka-25 [3]. The spectrum of Tunka-133 shows a number of features – deviations from the power law. Moreover one can treat the picture with such a manner that there is no power law at all, but the spectrum has a more complicated behaviour. The power law description can be used for small parts of the spectrum but for not more than half an order of magnitude. For an energy of about $2 \cdot 10^{16}$ eV the power law index changes from $\gamma = 3.23 \pm 0.01$ to $\gamma = 2.99 \pm 0.01$. This feature was first observed in the KASCADE-Grande experiment [8]. Points of the spectrum are consistent with such an index until energy $E_0 = 5 \cdot 10^{16}$ eV. Above this energy one notices a single point deflecting from the power law description to about 2 standard deviations. The energy of this point ($6.3 \cdot 10^{16}$ eV) coincides with that for the deflecting point observed in the GAMMA experiment [9]. Between this point and $E_0 = 3 \cdot 10^{17}$ the index is $\gamma = 3.07 \pm 0.03$. The spectrum becomes much steeper with $\gamma = 3.34 \pm 0.11$ above the last point (the second "knee").

In Fig. 8 the spectrum is compared with a number of other experimental data. The spectra of all the experiments shown in Fig. 8: KASCADE [10], EAS-TOP [11], Tibet [12], HEGRA [13] – are practically indistinguishable at the energy of the first (classical) knee.

There is agreement between the result of Tunka-133 and the spectra of GAMMA [9], KASCADE-Grande [8] and Ice-TOP [14] in the intermediate energy range 10^{16}–10^{17} eV. It should be noted that in Fig. 8 the differences among the spectra at E_0 about 10^{17} eV can be eliminated by correcting the energy by only 3%. Such an energy shift is much smaller than the absolute accuracy of these experiments.

For the highest energies Tunka-133 data agree with Fly's Eye [15], HiRes [16] and Telescope Array (TA) [17] data, and also, to a lesser extent, with Auger [18].

The fine structure of the spectrum in the range of 10^{15}–10^{17} eV does not contradict the so called rigidity dependent model of the knee origin [19]: any single galactic source providing the knee [20], accelerates particles up to a limited maximal energy depending on the charge of the nucleus Z, $E_{max}(Z) = Z \cdot E_{max}(Z = 1)$. In

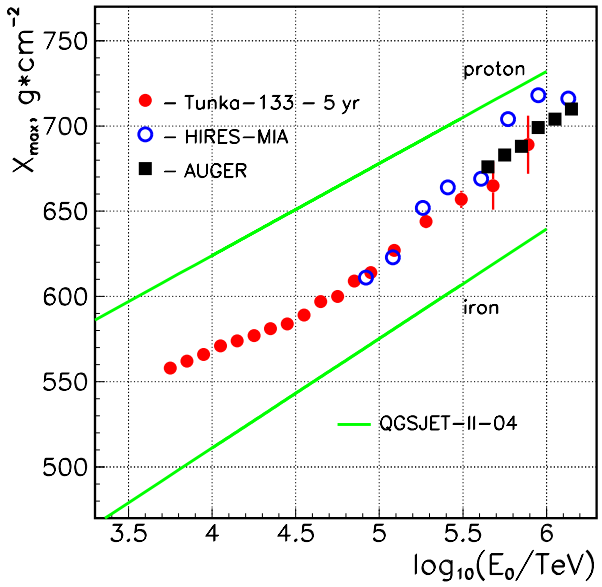

Figure 9. Mean experimental depth of maximum vs. the primary energy.

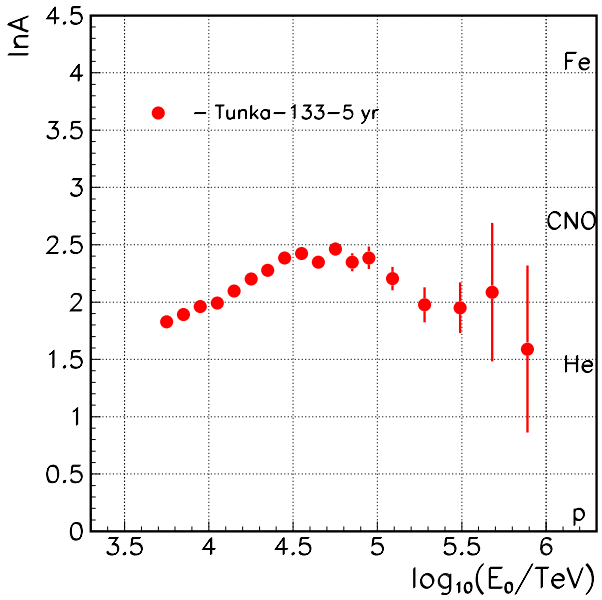

Figure 10. Mean logarithmic mass vs. the primary energy.

this interpretation the position of the first (classical) knee $3 \cdot 10^{15}$ eV corresponds to the proton cutoff, and the energy $6 - 8 \cdot 10^{16}$ eV indicates the cutoff for iron nuclei ($Z = 26$). The existence of more energetic particles can demand a discussion of new galactic sources of an unknown nature or (less probable) extragalactic sources.

5. The depth of maximum

The methods of EAS maximum depth X_{max} measurement are described in [4]. Events for this analysis are selected in a circle of radius 450 m. To get a uniform estimate for b_A over a wide range of energies, we remove from the analysis detectors at distances larger than 250 m from the core during the last step of parameters reconstruction. The experimental dependence of the mean $\langle X_{max} \rangle$ vs. primary energy E_0 in the energy range $6 \cdot 10^{15}$–10^{18} eV is shown in Fig. 9. The experimental points are compared with the points of the HiRes-MIA experiment [16] and fluorescent light detectors of the Pierre Auger Observatory [18]. One can see an agreement of the Cherenkov light Tunka experiment results with direct fluorescent light observations. The new measurements are compared with the theoretical curves simulated with the QGSJET-II-04 model for primary protons and iron nuclei.

The mean values of $\langle X_{max} \rangle$ can be recalculated to the mean values of $\langle \ln A \rangle$ by a simple method of interpolation. The result of such an approach for the points derived from the ADF steepness analysis are shown in Fig. 10. The primary mass composition becomes heavier in the energy range 10^{16}–$3 \cdot 10^{16}$ eV and lighter again in the range 10^{17}–10^{18} eV.

6. Conclusion

1. The primary CR energy spectrum in the range of $6 \cdot 10^{15}$–10^{18} eV has a number of features: the spectrum becomes harder (the index changes from $\gamma = 3.23 \pm 0.01$ to $\gamma = 2.99 \pm 0.01$) at $E_0 = 2 \cdot 10^{16}$ eV and steeper with an index $\gamma = 3.07 \pm 0.03$ at $E_0 = 6.3 \cdot 10^{16}$ eV and even steeper ($\gamma = 3.34 \pm 0.11$) at $E_0 = 3 \cdot 10^{17}$ eV.
2. In the energy range 10^{16}–10^{17} eV the observed Tunka spectrum is consistent with the spectra of KASCADE-Grande [8] and Ice-TOP [14].
3. Beyond the energy 10^{17} eV the Tunka-133 spectrum is consistent with fluorescent light experiments: Fly's Eye [15], HIRES [16] and hybrid experiment TA [17].
4. The depth of maximum X_{max} does not contradict the results obtained by fluorescent light experiments HiRes-MIA [16] and Auger [18].
5. The primary mass composition becomes heavier in the energy range 10^{16}–$3 \cdot 10^{16}$ eV and lighter again in the range 10^{17}–10^{18} eV.

This work was supported by the Ministry of Education and Science of the Russian Federation (State Contract 14.V25.31.0010, project 1366, zadanie N 3.889.2014/K), the Russian Foundation for Basic Research (grants 13-02-12095, 13-02-00214, 15-02-05769, 15-02-10005).

References

[1] Berezhnev S., *et al.*, (Tunka-133 Collaboration), Nucl. Instr. and Methods in Physics Research A **692**, 98 (2012)
[2] Antokhonov B.V., *et al.*, Nuclear Physics B (Proc.Suppl) **212–213** 53 (2011)
[3] Budnev N., *et al.*, Astropart. Phys. **50**, 18–25 (2013)
[4] Prosin V., *et al.*, Nucl. Instr. and Methods in Physics Research A **756**, 94 (2014)
[5] Prosin V.V. for the Tunka Collaboration, Nuclear Physics B (Proc.Suppl) **190** 247 (2009)
[6] Korosteleva E., *et al.*, Int. J. Mod Phys. A **20** 6837 (2005)

[7] Korosteleva E., *et al.* Nuclear Physics B (Proc. Supp.), **165** 74 (2007)
[8] Apel W.D., *et al.* (KASCADE-Gr. Collaboration), Astropart. Phys. **36**, 183 (2012)
[9] Garyaka A., *et al.*, Journal of Physics G: Nuclear and Particle Physics **ID=35**, 115201 (2008)
[10] Antony T., *et al.*, Nucl. Instr. and Methods in Physics Research A **513**, 490 (2003)
[11] Aglietta M., *et al.*, EAS-TOP Collaboration, Astropart. Phys. **10**, 1 (1999)
[12] Amenomori M., *et al.*, (Tibet Col.), Astrophys. J, **678**, 1165 (2008)
[13] Arqueros F., *et al.*, The HEGRA Collaboration, Astron. Astrophys. **359**, 682 (2000)
[14] Aartsen M.G., *et al.*, Phys. Rev. Lett. D **88**, 042004 (2013)
[15] Abu-Zayyad T., *et al.*, Phys. Rev. Lett. **84**, 4276 (2000)
[16] Sokolsky P. for the HiRes Collaboration, Nuclear Physics B (Proc. Suppl.) **212–213**, 74 (2011)
[17] Abu-Zayyad T., *et al.*, Astropart. Phys. **48**, 16 (2013)
[18] Schulz A. for the Pierre Auger Collaboration, Proc. 33rd ICRC Rio De Janeiro **ID=769** (2013)
[19] Sveshnikova L.. *et al.*, Nuclear Physics B (Proc. Suppl.) **218–224**, 256 (2014)
[20] Erlykin A., Wolfendale A., Martirosov R., CERN-Courier **21**, 201 (2011)